Steady Baroclinic Flow through Ridges with Narrow Gaps*

J. PEDLOSKY

Woods Hole Oceanographic Institution, Woods Hole, Massachusetts

(Manuscript received 17 October 2000, in final form 23 January 2001)

ABSTRACT

The steady baroclinic flow in a basin containing a meridional barrier representing a midocean ridge is studied in the linear, quasigeostrophic limit of a two-layer model. Thermal damping and a simple friction provide dissipation of thickness (heat) and momentum. The ridge is pierced by two gaps in the upper layer but only a single gap in the lower layer. The flow in the model is forced by specified upwelling at the upper surface and by a specified cross-isopycnal velocity at the interface in addition to the autogenerated cross-isopycnal velocity associated with the thermal damping. The forcing may be either broad in longitude or narrowly confined.

The nature of the geometry of the model ridge mixes the baroclinic and barotropic response to the forcing, and this has profound consequences for the resulting circulation. In particular, when the baroclinic interaction of the two layers is strong, the recirculation region to the east of the ridge, previously discovered in earlier barotropic models of the circulation, grows in meridional extent so that the flow along the ridge segment may be unidirectional along the ridge. It is suggested that the theory may explain observations of such flow in the Angola Basin, which appeared previously to violate an application of Kelvin's theorem.

The theory also predicts zonal jets west of the gaps in the ridge, spreading meridionally with distance from the ridge. The jets are strongly barotropic whether the external forcing is baroclinic or barotropic.

1. Introduction

The presence of midocean ridges adds new elements to the character of the oceanic general circulation. In particular, the presence of gaps in the midocean ridges allows for the communication through the ridges of even deep flows between contiguous ocean subbasins. In many cases the islandlike character of the ridge in the interval between the gaps adds complicating dynamical factors to the standard circulation theory. For example, in their discussion of the deep flow in the Angola Basin of the South Atlantic, Warren and Speer (1991, hereafter WS) attempt to apply classical Stommel–Arons theory to the flow but the ''island'' formed by the intragap ridge segment adds an element of apparent indeterminacy to the calculation.

From a theoretical point of view, the presence of such islands has led to the formulation of theories to deal with the non-simply connected region formed by the isolated ridge segment and to resolve the indeterminacy alluded to above. The work of Godfrey (1989) and Pedlosky et al. (1997, hereafter PPSH) attempts to resolve the ambiguity introduced by the ''hole'' in the fluid produced by the island by an application of Kelvin's theorem to a contour coincident with the island's boundary. In PPSH the circulation of a barotropic fluid around such islands was studied theoretically and experimentally, and one of the chief consequences of the theory is the prediction of a recirculation region in the linear limit for the region of flow just east of the isolated ridge segment. The recirculation arises since Kelvin's theorem demands that in the steady state the integral of the tangential component of the frictional force must vanish when integrated around the island. Since for steady flows of planetary scale the major currents appear on the *eastern* sides of such islands, the condition reduces to the requirement that the tangent component of the frictional force has zero average when integrated over the meridional length of the segment between the two gaps on the eastern side. For motion governed by linear dynamics this normally implies that the integral of the velocity itself must vanish when integrated over the eastern stretch of the island or ridge segment. The recirculation results if the Sverdrup flow has a zonal velocity of two signs over the meridional extent of the segment; otherwise no recirculation arises, but a single stagnation point appears along the segment so that the flow is of opposite signs on different portions of the segment. These results were verified for the barotropic case by both laboratory and numerical experiments in PPSH. Indeed, this basic constraint forms an element

* Woods Hole Contribution Number 10371.

Corresponding author address: Dr. J. Pedlosky, Physical Oceanography, Woods Hole Oceanographic Institution, Clark 363, MS21, Woods Hole, MA 02543.
E-mail: jpedlosky@whoi.edu

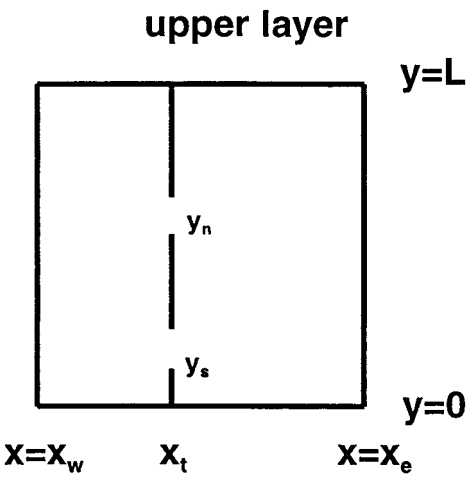

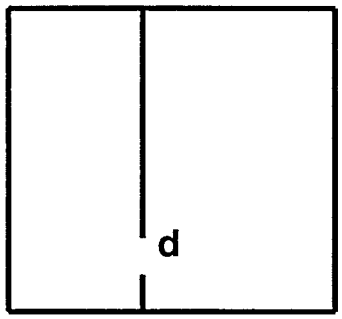

lower layer

FIG. 1. The geometry of the two-layer model. The ridge at $x = x_t$ in the upper layer has two gaps of width d. The gaps are in the intervals $y_s < y < y_s + d$ and $y_n - d < y < y_n$. The lower-layer ridge has a single gap in the interval $y_s < y < y_s + d$/ It is assumed that $d \ll L$. The meridional extent of the basin is L and its eastern and western boundaries are at x_e and x_w.

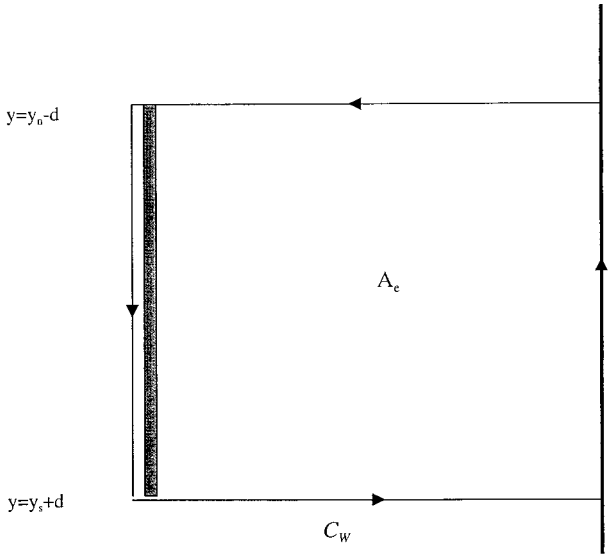

FIG. 2. The contour used to calculate the island constant. The contour is shown slightly displaced from the western side of the ridge segment for clarity. In actuality, it coincides with the western boundary of the ridge segment.

of Godfrey's ''Island Rule,'' which also holds for the barotropic Sverdrup transport in the linear limit.

However, in their investigation of the flow on the eastern flank of the Mid-Atlantic Ridge, WS found flow in the upper layer of the abyssal region that was unidirectional (see their Fig. 4) in a depth interval for which the ridge was bounded on the north and south by gaps, and indeed they conclude their paper with the remark, referring to the Kelvin constraint, ''The frictional argument seems ineluctable, but it also seems to fail. Why?'' That question forms a major part of the motivation of the present study.

In the situation studied by WS the flow was baroclinic and the geometry of the ridge was such that only the upper layer, in this region, was islandlike, while the lower layer(s) had, at most, a single entry-port into the Angola Basin. In this paper we will consider the baroclinic flow of a two-layer region that has that geometrical property.

Figure 1 shows the geometry of the model. A rectangular ocean basin is essentially bisected by a barrier representing the ridge. The model is imagined as a model just for the abyssal circulation. In the upper layer of the model the ridge is pierced by two gaps of width d in the intervals $y_s < y < y_s + d$ and $y_n - d < y < y_n$. An assumption of the analysis, which simplifies the calculation, is the realistic one that $d \ll L$ where L is a characteristic large scale of the basin and the forcing. The flow in the model will be driven by a specified upwelling at the upper boundary and by a specification of the cross-isopycnal mass flux at the interface between the two layers. The formulation of the model is described in detail in section 2. Section 3 deals with the general integral constraints that obtain. There are two. The integral of the tangential component of the momentum equation around the contour bounding the isolated segment of the ridge in the upper layer, a version of Kelvin's theorem, leads to a fundamental constraint on the nature of the flow. It, along with the condition of mass conservation in the lower layer (McWilliams 1977), are sufficient to determine the two important free parameters of the problem, which arise in quasigeostrophic theory. They are 1) the constant value of the upper-layer streamfunction on the island segment, Ψ_I, and 2) the constant value of the streamfunction on the outer boundary of the basin in the lower layer, Ψ_2. The value of the streamfunction on the outer boundary of the basin in the upper layer can be chosen without loss

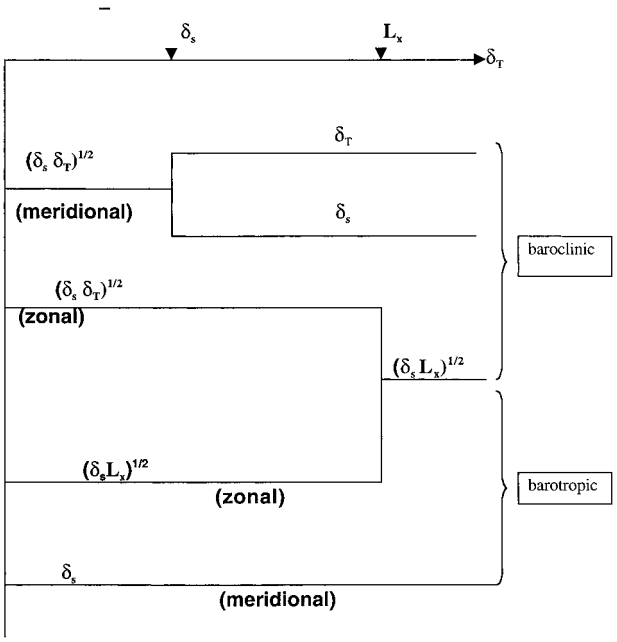

FIG. 3. Schematic showing the behavior of the widths of the barotropic and baroclinic boundary layers as a function of δ_T. At the two critical lengths, L and δ_s, the boundary layers may split or coalesce. Note that for small enough δ_T the baroclinic boundary layers have the same scale $(\delta_s\delta_T)^{1/2}$ on all boundaries.

of generality to be zero. Thus, Ψ_2 determines the uniform thickness perturbation due to the motion on the outer boundary, while Ψ_I represents the geostrophic mass flux though the gaps in the upper layer. It is especially important to note that the boundary values of the streamfunctions in each layer extend to the portions of the ridge in contact with the basin boundary. In section 4 the solution to the linear problem is described. The incompleteness of the gaps in the lower layer mixes the barotropic and baroclinic responses to the forcing, and this has important consequences for the structure of the resulting flow and the nature of the recirculation produced in the eastern sub-basin. Such a mode mixing is also seen in the problem of Rossby wave transmission past barriers of this type (Pedlosky 2000). Section 5 discusses the results of the calculations based on the theory and, in particular, focuses on the role of the baroclinicity in coupling the two layers, altering the structure of the eastern basin recirculation cell and the strong zonal jets produced in the western sub-basin at the latitudes of the upper-layer gaps. Section 6 concludes with an overall summary of the results with some remarks directed to possible observational evidence for the jets.

Although the primary motivation for this study is the aforementioned abyssal circulation near the midocean ridge, the model clearly also applies to the wind-driven circulation around large islands and emphasizes the im-

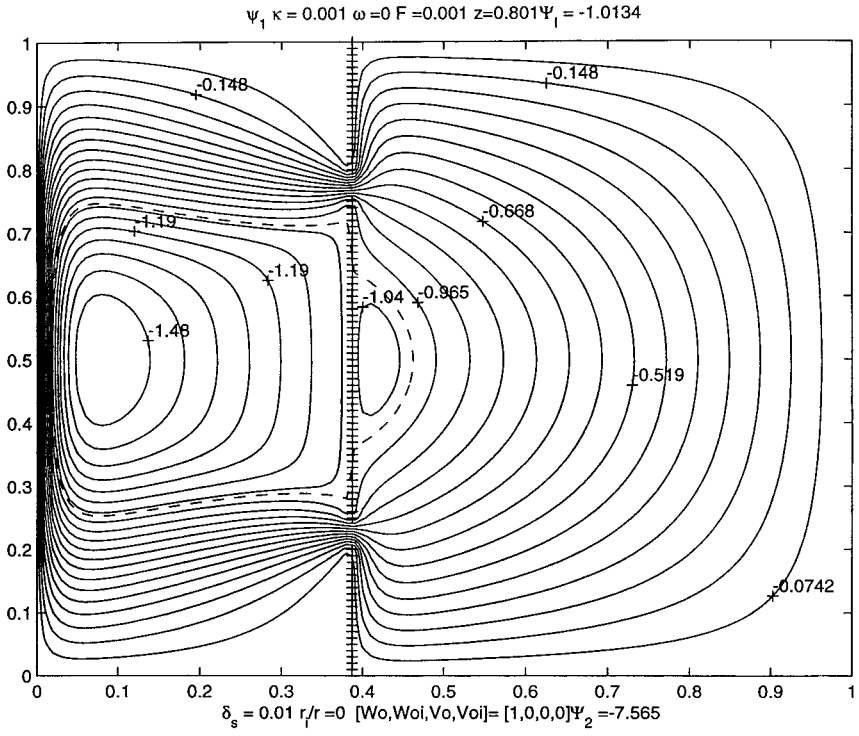

FIG. 4. The circulation pattern in the upper layer for the case of forcing by a smooth upwelling at the upper surface and the absence of interfacial coupling. In this example $r_I = 0$, and κF is very small. The circulation is limited to the upper layer and the pattern reproduces the recirculation region of a barotropic model.

portant role that mixing in regions close to the boundaries may play in affecting the large-scale circulation in the vicinity of the island and its interaction with the large-scale circulation.

2. Model formulation

Although the basic model to be employed is the classical two-layer quasigeostrophic model, details of the momentum equation within that implied expansion must be carefully used in the calculation, so it is helpful to briefly review the fundamentals of the model.

For each layer the variables are subscripted with $n = 1$ referring to the upper layer and $n = 2$ for the lower layer. The momentum equations employed in this study are

$$b\frac{\partial \mathbf{u}_n}{\partial t} + \mathrm{Ro}\mathbf{u}_n \cdot \boldsymbol{\nabla}\mathbf{u}_n + f\mathbf{k} \times \mathbf{u}_n = -\boldsymbol{\nabla}p_n - \left(\frac{r}{f_o h_n^*}\right)\mathbf{u}_n - \left(\frac{r_i}{f_o h_n^*}\right)(-1)^n(\mathbf{u}_1 - \mathbf{u}_2). \tag{2.1}$$

In (2.1) all variables are dimensionless with the exception of the layer thickness h_n^*. Time has been scaled with βL, the horizontal velocities with U, and the pressure with $\rho_o f_o UL$, where ρ_o is the mean density of the two layers and f_o is the value of the Coriolis parameter at $y = 0$ (the southern boundary of the basin). The parameters appearing in (2.1) are $b = \beta L/f_o$, supposed small for the beta-plane assumption, and $\mathrm{Ro} = U/f_o L$, which measures the nonlinearity in the momentum equation. The friction terms are represented by simple drag laws. The second term on the right-hand side of the equation yields a Stommel-like drag law proportional to the layer velocity itself with a drag coefficient r, while the final term represents a frictional interaction between the two layers whose coefficient is r_i. Lateral mixing of momentum could be included with no fundamental change in the results to be discussed. The Coriolis parameter in (2.1) is $f = 1 + by$ and both the x and y variables are scaled with L, the meridional scale of the basin.

The layer thickness may be written

$$h_n^* = H_n(1 + \mathrm{Ro}F_n h_n) \tag{2.2a}$$

$$F_n \equiv \frac{f_o^2 L^2}{g' H_n}, \tag{2.2b}$$

where g' is the reduced gravity based on the density difference between the two layers and H_n is the layer thickness of each layer in the absence of motion. The scaled variable h_n describes the variation of the layer thickness due to the motion. The parameters F_n are assumed to be $O(1)$ for the purposes of the expansion.

The continuity of pressure and the hydrostatic relation require that

$$h_n = (-1)^n(p_2 - p_1). \tag{2.3}$$

The integrated equation for mass continuity in each layer is

$$bF_n\frac{\partial h_n}{\partial t} + \mathrm{Ro}F_n\mathbf{u}_n \cdot \boldsymbol{\nabla}h_n + (1 + \mathrm{Ro}F_n h_n)\boldsymbol{\nabla} \cdot \mathbf{u}_n = -b\kappa F_n h_n - b\left[\frac{H}{H_n}\right]((-1)^n W_* + w_e\delta_{n1}). \tag{2.4}$$

In (2.4) the right-hand side represents the effect of the cross isopycnal velocities in each layer. The first term on the right-hand side represents a thermal damping term proportional to the displacement of the interface with a time constant for decay equal to $\beta L\kappa$ in dimensional units. The functions W_* and w_e are, in addition, specified forcing terms representing imposed cross-isopycnal velocities at the interface, W_*, and at the upper surface where the velocity is labeled w_e in analogy with Ekman pumping. These vertical velocities are scaled with W_o where the horizontal and vertical scales for the velocity are related by

$$U = \frac{f_o W_o}{\beta H}. \tag{2.5}$$

These imposed velocities represent potential vorticity sources in addition to the thermal and frictional dissipation terms in Eqns. (2.1) and (2.4); H is the total mean depth $H_1 + H_2$, which is taken to be constant in this study.

A standard expansion of the equations in an asymptotic series in the beta plane parameter b leads to the following momentum, mass and vorticity balances, where superscripts denote the order in the b expansion:

$$\mathbf{u}_n^{(o)} = \mathbf{k} \times \boldsymbol{\nabla}\psi_n \tag{2.6a}$$

$$\frac{\partial}{\partial t}q_n + \delta_I^2\mathbf{u}_n^{(o)} \cdot \boldsymbol{\nabla}q_n + \frac{\partial \psi_n}{\partial x} = \frac{1}{\hat{h}_n}[w_e\delta_{n1} + (-1)^n W_*] - F_n\kappa(-1)^n(\psi_2 - \psi_1) - \frac{\delta_s}{\hat{h}_n}[\nabla^2\psi_n + (-1)^n r_i/r\nabla^2(\psi_2 - \psi_1)] \tag{2.6b}$$

$$q_n = \nabla^2\psi_n + F_n(-1)^n(\psi_1 - \psi_2) \tag{2.6c}$$

In (2.6b)

$$\delta_I^2 = \frac{U}{\beta L^2} \tag{2.7a}$$

$$\delta_s = \frac{r}{H\beta L} \tag{2.7b}$$

$$\hat{h}_n = \frac{H_n}{H}, \tag{2.7c}$$

which are the scaled inertial and Stommel boundary

layer widths of classical circulation theory and the fractional layer depths in the absence of motion.

The momentum and mass equations, needed below, at $O(b)$ are simply

$$\frac{\partial \mathbf{u}_n^{(o)}}{\partial t} + \delta_I^2 \mathbf{u}_n^{(o)} \cdot \nabla \mathbf{u}_n^{(o)} + \hat{k} \times (\mathbf{u}_n^{(1)} + y\mathbf{u}_n^{(o)}) = -\nabla p_n^{(1)} - \frac{\delta_s}{\hat{h}_n}[\mathbf{u}_n^{(o)} + (-1)^n r_i/r(\mathbf{u}_2^{(o)} - \mathbf{u}_1^{(o)})] \quad (2.8)$$

$$\nabla \cdot \mathbf{u}_n^{(1)} + F_n\left[\frac{\partial h_n^{(o)}}{\partial t} + \delta_I^2 \mathbf{u}_n^{(o)} \cdot \nabla h_n^{(o)}\right] = \frac{-1}{\hat{h}_n}[w_e \delta_{n1} + (-1)^n W_*] - \kappa F_n h_n^{(o)}. \quad (2.9)$$

The zero-order velocities are horizontally nondivergent, but the higher-order velocities possess a divergence and enter into the mass budget that must be satisfied for the basin as a whole. I will assume that, except at specified sources and sinks on the boundaries of the basin, both the zero- and first-order velocities have zero normal component at solid boundaries.

On the outer boundary of the basin the streamfunction must be constant in each layer. In the upper layer we may take the value of that constant to be zero without loss of generality. In the lower layer that constant, which must be determined, will be designated Ψ_2. On the ridge segment in the upper layer, which is not connected to the outer boundary, the streamfunction is again constant and a priori unknown, and is called Ψ_I.

3. Integral constraints

If the component of (2.8) tangent to the segment of the ridge is integrated around the ridge segment and if the normal velocity at both $O(1)$ and $O(b)$ are assumed to vanish on the ridge, we obtain

$$\frac{\partial}{\partial t}\oint_{C_I} \mathbf{u}_1^{(o)}\, d\mathbf{s} = -\frac{\delta_s}{\hat{h}_1}\oint_{C_I} [\mathbf{u}_1^{(o)} + r_i/r(\mathbf{u}_1^{(o)} - \mathbf{u}_2^{(o)})]\, d\mathbf{s}, \quad (3.1)$$

where C_I is the contour that girdles the ridge segment and the integration proceeds in a counterclockwise path around the segment. Note that the Coriolis and nonlinear advection terms identically vanish as long as the velocity has no normal component to the segment. In the steady state the left-hand side of (3.1) is identically zero and the circulation condition involves only the integral of the velocity and, in the presence of frictional coupling between the layers, the integral of the shear between the two layers. When that coupling is zero, (3.1), in the steady state, reduces to the condition that the average of the tangential component of velocity, when integrated around the segment, must be zero. If the major currents are on the eastern side of the island, this leads to the condition that the average meridional velocity on the eastern side of the segment must be zero and at least one stagnation point on the eastern side of the ridge must exist. When the frictional coupling is nonzero, this is no longer true. In fact, in the limit when $r_i/r \gg 1$ the steady condition simply reduces to the statement that the average value of the velocities must be the same in each layer. Since the lower layer's portion of the ridge is attached to the boundary, there is no constraint similar to (3.1) for the lower layer and the lower-layer meridional velocity need not have a zero average, which seems to imply that, at least in the case $r_i/r \gg 1$, the upper-layer velocity could be unidirectional along the ridge. What is not so obvious, and what will be seen below, is that this can also occur when $r_i/r = 0$ with sufficient baroclinic coupling.

The second constraint concerns the conservation of mass of the lower layer. The single gap in the barrier will strongly impede mass flux between the two subbasins for the $O(1)$ flow, but the mass balance depends on the integral of the $O(b)$ mass conservation condition expressed by (2.9). When (2.9) is integrated over the area of the total basin the condition of mass conservation leads to the constraint

$$\iint_A W_*\, dx\, dy + F_2\hat{h}_2\left[\kappa + \frac{\partial}{\partial t}\right]\iint_A h_2^{(o)}\, dx\, dy = S_2 - \delta_I^2 F_2 \hat{h}_2 \oint_{C_B} h_2^{(o)}\mathbf{u}_2^{(o)} \cdot \mathbf{n}\, ds. \quad (3.2)$$

Here C_B is the contour encircling the boundary of the lower layer in the basin. The number S_2 is the net input of mass into the second layer through the lateral boundary by the $O(b)$ motion field, that is,

$$S_2 = -\hat{h}_2 \oint_{C_B} \mathbf{u}_2^{(1)} \cdot \mathbf{n}\, ds, \quad (3.3)$$

and where $\mathbf{n}$ is the outward normal to the boundary. In the steady state, since no temporary storage is possible, the condition (3.2) expresses the condition that the net $O(b)$ flow entering through the lateral boundaries must exit through the interface into the upper layer. Note that there can be no *net* quasigeostrophic flow entering the lower layer due to the condition that ψ_2 be single valued.

It is the application of these two conditions that determine the two constants Ψ_I and Ψ_2. Godfrey (1989) showed how, under the conditions that certain simplifications obtain, the constant Ψ_I could be determined directly from the forcing fields. Without repeating essentially the same derivation found in his paper it is straightforward to show that, starting from the $O(b)$ momentum and mass equations in the upper layer, one can derive

$$(y_n - y_s - 2d)\Psi_I = -\frac{1}{\hat{h}_1}\iint_{A_e}(w_e - W_*)\,dx\,dy + \frac{\delta_s}{\hat{h}_1}\oint_{C_w}[\mathbf{u}_1^{(o)} + r_i/r(\mathbf{u}_1^{(o)} - \mathbf{u}_2^{(o)})]$$

$$+ \frac{F_1}{\hat{h}_1}\kappa\iint_{A_e} h_1^{(o)}\,dx\,dy + \delta_I^2\oint_{C_w}\mathbf{u}_1^{(o)}q_n\cdot\mathbf{n}\,ds. \tag{3.6}$$

In (3.6) the contour C_w runs (see Fig. 2) from the eastern boundary along a latitude circle at the northern tip of the segment, south along the *western side* of the segment, to the eastern boundary along the latitude line coincident with the southern tip of the segment, and then northward along the eastern boundary to close on itself. The area A_e is the area to the *east* of the segment enclosed by the contour and **n** is the outward normal to the contour. When dissipation and nonlinearity can be ignored everywhere except on the eastern side of the segment (where strong ''western'' boundary currents are expected), all the terms in (3.6) can be ignored except the first terms on the right-hand side and a simple expression for the streamfunction on the ridge segment. In the linear limit the determination is equivalent to what is obtained from (3.1). Of course, it is only after the solution is in hand that one can be sure that such terms can be neglected, and we proceed to examine the solution in detail in the next section. We shall find that, when the baroclinicity is important, several of these conditions, in particular, ignoring the velocity on the western side of the ridge in either (3.1) or (3.6) are no longer valid.

4. Linear problem

We consider, for simplicity, the linear problem. Although the nature of the topography will mix the baroclinic and barotropic responses to the forcing, it is efficient and revealing to consider the problem for the barotropic and baroclinic responses separately to the extent possible. We define the barotropic and baroclinic geostrophic streamfunctions as

$$\psi_B = \hat{h}_1\psi_1 + \hat{h}_2\psi_2, \tag{4.1a}$$

$$\psi_T = \psi_1 - \psi_2. \tag{4.1b}$$

By manipulating (2.6a,b) in the standard way and ignoring the nonlinear terms proportional to δ_I^2 we obtain the following linear equation for the barotropic and baroclinic stream functions:

$$\frac{\partial}{\partial t}\nabla^2\psi_B + \frac{\partial\psi_B}{\partial x} = w_e - \delta_s\nabla^2(\psi_1 + \psi_2). \tag{4.2}$$

We note that the right-hand side of (4.2) cannot in general be written in terms of only the barotropic streamfunction. The frictional terms, whose forms are rather artificial, will mix barotropic and baroclinic modes of motion unless the layer thicknesses in the absence of motion are equal. It would be preferable to have such mode mixing be due to a robust physical feature of the model, such as the nature of the topography, rather than the representation of the friction. To avoid that mode mixing by friction I will restrict attention to the case for which $\hat{h}_1 = \hat{h}_2 = ½$. Then (4.2) becomes

$$\left(\frac{\partial}{\partial t} + 2\delta_s\nabla^2\right)\psi_B + \frac{\partial\psi_B}{\partial x} = w_e, \tag{4.3}$$

while the equation for the baroclinic response becomes

$$\frac{\partial}{\partial t}[\nabla^2\psi_T - 2F\psi_T] + 2\delta_s\left(\nabla^2\psi_T - \frac{\kappa F}{2\delta_s}\psi_T\right)$$

$$+ 4\left(\frac{r_i}{r}\right)\delta_s\nabla^2\psi_T + \frac{\partial\psi_T}{\partial x} = 2w_e - 4W_*. \tag{4.4}$$

Here,

$$F = F_1 + F_2 = \frac{f_o^2L^2}{H_1H_2}H.$$

For the steady-state problem the time derivative is, of course, zero but it is retained in (4.3) and (4.4) to emphasize the similar roles of time dependence and dissipation in the model.

On the external boundaries of the basin the boundary conditions are

$$\psi_B = \hat{h}_2\Psi_2 = \frac{1}{2}\Psi_2, \qquad \psi_T = -\Psi_2. \tag{4.5}$$

These conditions hold also on the portion of the ridge connected to the outer boundary.

We now exploit the narrowness of the gaps in the ridge. On the isolated ridge segment in the upper layer the streamfunction is a constant and equal to Ψ_I, while on the portions of the ridge connected to the basin boundary the streamfunction is zero. As in Pedlosky and Spall (1999), we assume that in the narrow interval between the ridge and its segment connected to the outer boundary the streamfunction varies linearly from zero to Ψ_I. Pedlosky and Spall checked this assumption by direct numerical integration and found it valid when, as

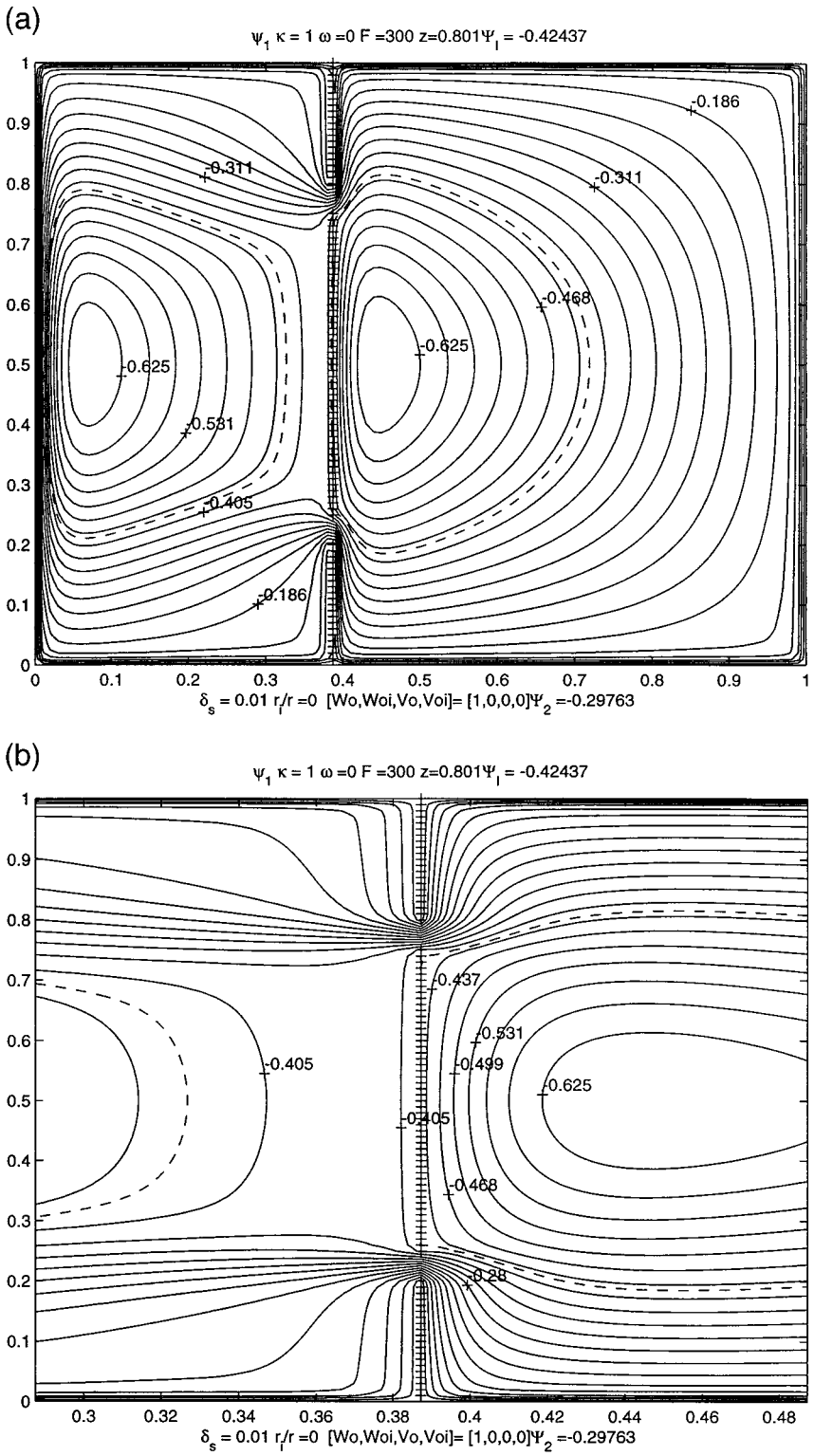

FIG. 5. For the parameter setting $r_I = 0$, $\kappa F = 300$, $\delta_s = 0.01$, for the same forcing as in Fig. 4. (a) The circulation in the upper layer. Note that the dashed curve outlining the recirculation region covers the whole ridge segment between the gaps. (b) A close-up of the upper-layer circulation pattern near the ridge demonstrating the existence of a meridional flow west of the ridge.

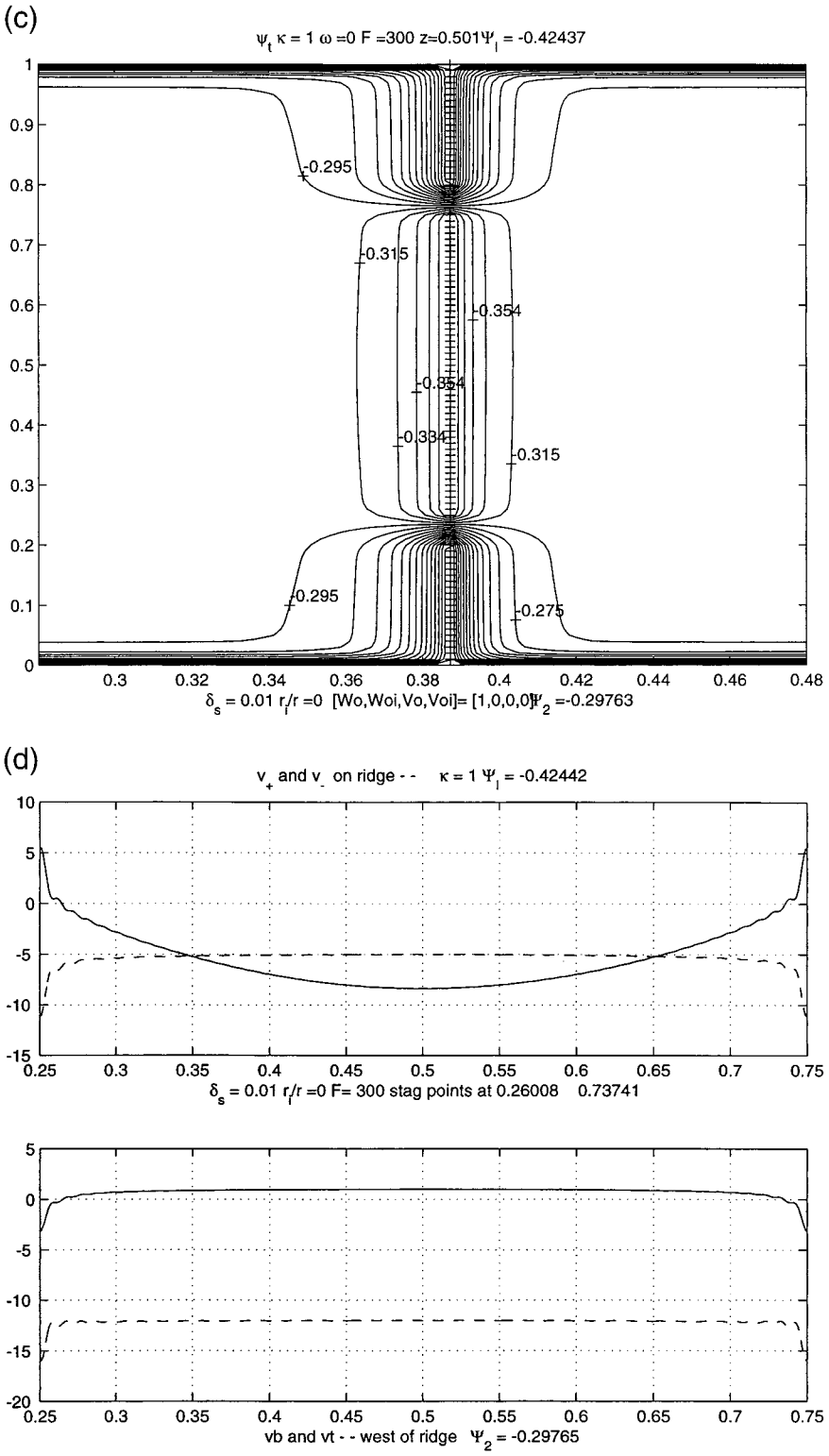

FIG. 5. (*Continued*) (c) The baroclinic streamfunction in the vicinity of the ridge illustrating the symmetric boundary layer structure. The function contoured is the difference between ψ_T and its boundary value Ψ_T. (d) Upper panel shows the meridional velocity along the ridge segment; the solid curve is for v east of the ridge and the dashed curve is for v west of the ridge. The lower panel shows (solid) the weak barotropic velocity to the west of the ridge, and the dashed curve shows the strong baroclinic velocity to the west of the ridge.

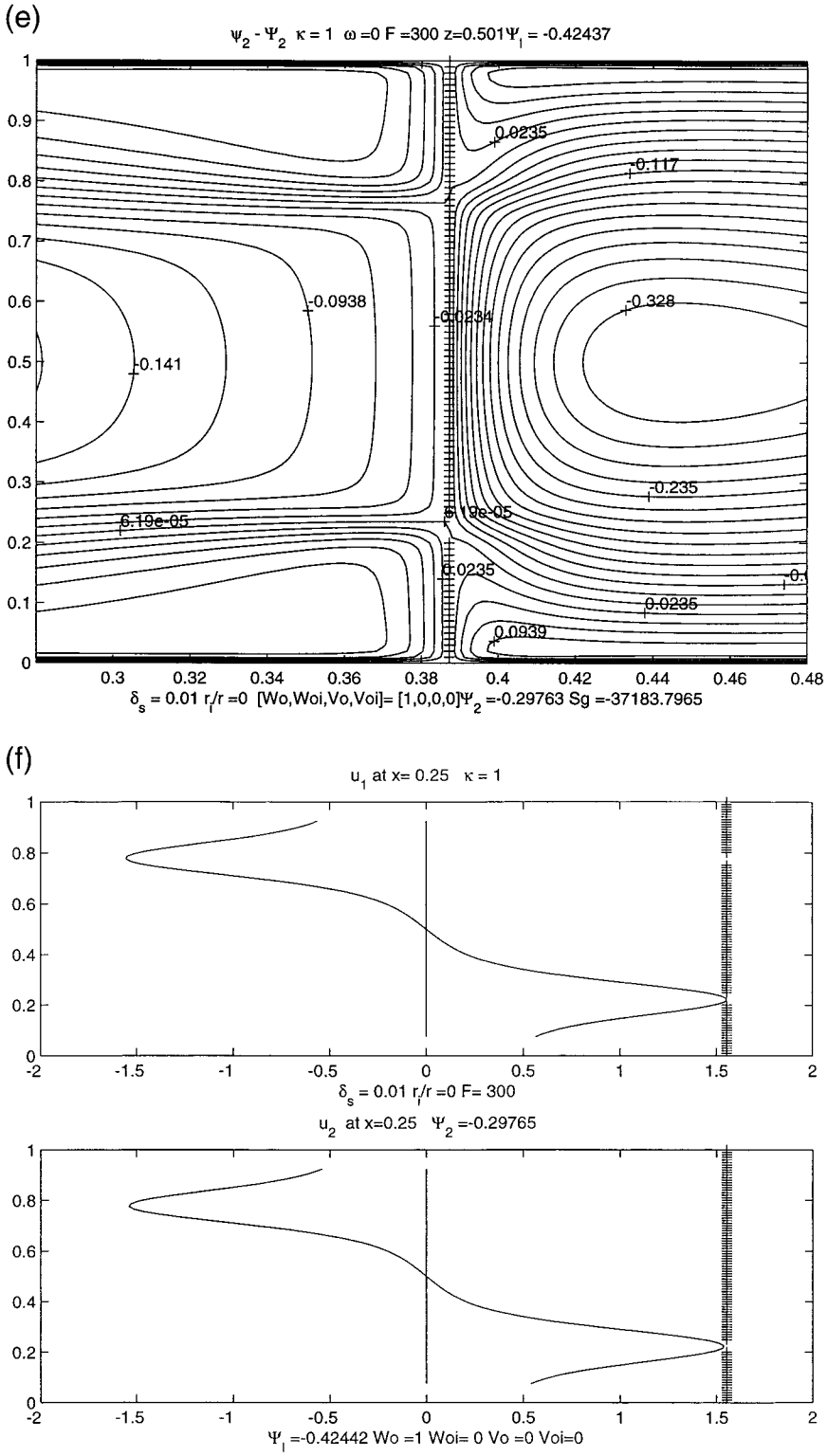

FIG. 5. (*Continued*) (e) The circulation in the lower layer in the vicinity of the ridge. (f) The profiles of the zonal velocity in the upper layer (upper panel) and lower layer (lower panel) at a position ($x = 0.25$) west of the ridge.

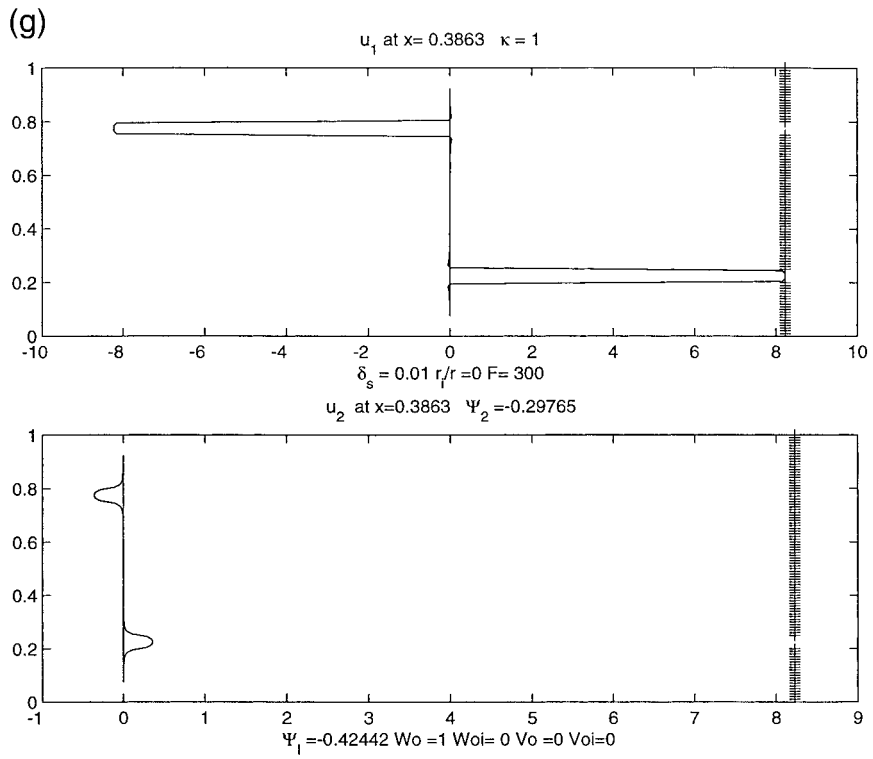

FIG. 5. (*Continued*) (g) The same zonal velocity profiles just west of the ridge, showing that the lower-layer zonal velocity goes to zero at the ridge.

in the present case, $d \ll 1$. Thus on the longitude of the ridge at $x = x_t$, it follows that

$$\psi_1 = \Psi_I \begin{cases} 0, & 0 < y < y_s \\ (y - y_s)/d, & y_s < y < y_s + d \\ 1, & y_s + d < y < y_n - d \\ (y_n - y)/d, & y_n - d < y < y_n \\ 0, & y_n < y < 1. \end{cases} \quad (4.6)$$

This has important implications for the flow in the lower layer. A similar approximation implies that there is no $O(1)$ quasigeostrophic flow through the single gap in the lower layer, since the streamfunction on all portions of the ridge in the lower layer, and, thus on each side of the gap, is equal to Ψ_2. Nevertheless, it will be possible to deduce the net $O(b)$ flow through that gap as shown below. That condition and (4.6) can easily be written in terms of the barotropic and baroclinic components to establish the appropriate boundary condition on the ridge segment, a step which is deleted for the sake of brevity.

Before describing the method of solution in detail it is useful to review the character of the boundary layer structures that obtain from (4.3) and (4.4) in the limit of small dissipation. Boundary layer theory, per se, will not be used in the calculation, but its results are most easily interpreted with the asymptotic structure of the boundary layers kept in mind. For the linear problem defined by (4.3) and (4.4) it is straightforward to deduce the boundary layer balances. They differ for the barotropic and baroclinic modes and differ for boundary layers on the meridional and zonal boundaries.

For the barotropic mode of motion, the boundary layers on the meridional boundaries will have the Stommel length scaled δ_s for all values of the stratification. On zonal boundaries or internal boundary layers that coincide with a latitude circle the length scale is $(\delta_s L_x)^{1/2}$, where L_x is a characteristic dimensionless distance in the x direction. The governing equation for this layer is the diffusion equation in which $-x$ plays the role of the time variable and the solution parabolically spreads in y with increasing distance westward regardless of the direction of the flow as discussed in detail in PPSH. This will determine the structure of the zonal jets, which are tied to the gaps in the ridge and form the means of communication between the adjacent sub-basins.

For the baroclinic motion there is an additional scale that must be considered, and this is the baroclinic scale (Kawase 1987). In our dimensionless units this is

$$\delta_T = (\kappa F)^{-1}. \quad (4.7)$$

In dimensional units this scale is just the length a long, baroclinic Rossby wave can propagate westward before thermal damping dissipates it.

For large values of δ_T, that is, for small values of κ or F, the boundary layer structure for the baroclinic

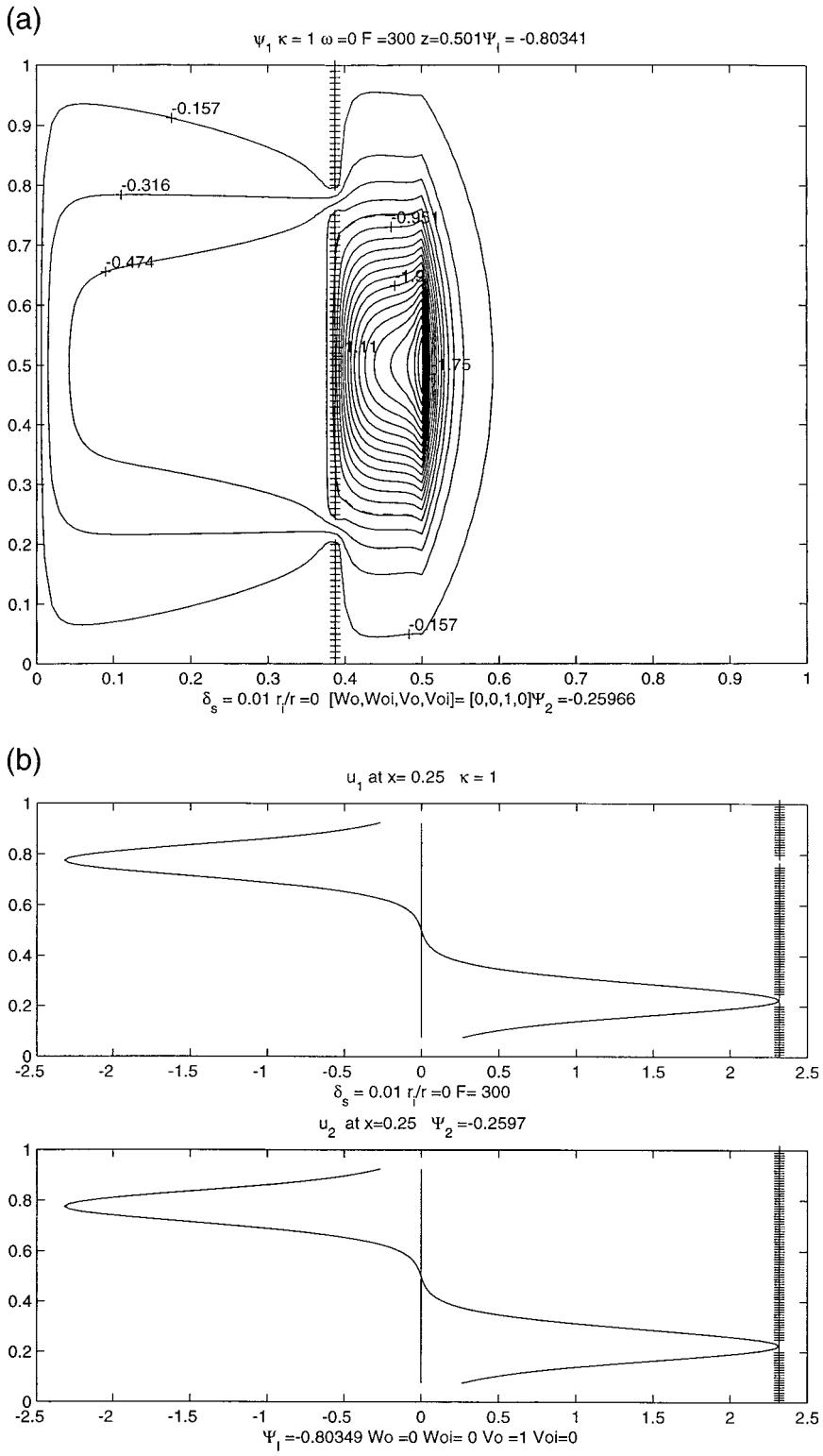

FIG. 6. The circulation induced by a zonally localized forcing. In this case there is an upwelling concentrated at $x = 0.5$ at the upper surface for the parameter setting $r_I = 0$, $\kappa F = 300$, $\delta_s = 0.01$. (a) The circulation in the upper layer. (b) The zonal velocity profiles in the two layers at $x = 0.25$.

mode is as follows. On meridional boundaries there is a western boundary layer scale, which is again the Stommel scale δ_s. In the vicinity of the eastern boundary there will be a zone in which the decaying Rossby wave is manifest and this will introduce a scale δ_T to the baroclinic zone near the eastern boundary. This region may, indeed, be very broad and it is sometimes included in the interior baroclinic solution. However, as κF increases, the eastern scale diminishes. When δ_T becomes as small as the Stommel scale, the boundary layer balances change in (4.4) and the baroclinic layers on both the eastern and western boundaries become equal and have the scale $(\delta_s\delta_T)^{1/2}$. In this limit the boundary layer scales are similar to linear coastal upwelling layers on an f plane; that is, β plays no role and there is symmetry between east and west. On zonal boundaries the scale for the baroclinic solution is $(\delta_s L_x)^{1/2}$ for large δ_T and the governing equation is the same diffusion equation as in the barotropic case. However, when δ_T becomes smaller than the basin scale, that is, $\delta_T < L$, the boundary layer equation becomes identical to the balance obtained for the meridional scale for large F, that is, $(\delta_s\delta_T)^{1/2}$. Thus, when κF is large enough the baroclinic boundary layer on *all* boundaries has this scale and there is a fundamental symmetry between east and west that is lacking in the barotropic mode. In this limit the governing boundary layer equation occurs as a balance of the terms in the second bracket on the left-hand side of (4.4), that is, a balance between frictional and thermal dissipation. Figure 3 shows the morphology of the boundary layer scales as a function of the baroclinic scale δ_T and shows the splitting of the boundary layer scales as the critical values δ_s and L are obtained. The baroclinic boundary layers may not, in the large F limit, carry much transport but they are important contributors to the dissipation integral in the circulation condition (3.1). The fact of the east–west symmetry in the large F limit (when the deformation radius is small with respect to the basin scale) will be seen to imply that the dissipation on the western side of the ridge can no longer be ignored for $O(1)$ κ, and this vitiates the validity of the island rule.

As remarked above, it is not necessary to use the approximations of boundary layer theory to solve the linear problem. Indeed, since we will be interested in the change in structure as a function of increasing stratification, it is more efficient to have a solution valid for a wide range of parameters.

Although we are interested in the response to steady forcing, it is just as easy to consider the solution as a response to a periodic forcing at frequency ω_o although we consider in this paper only the solutions for that forcing frequency equal to zero.

Defining

$$\omega_B = \omega_o - 2i\delta_s,$$
$$\omega_T = \omega_o - 2i\delta_s(1 + 2r_i/r), \tag{4.8}$$

the governing equations for the barotropic and baroclinic parts of the flow can be written as

$$\nabla^2\psi_B - 2ik_B\frac{\partial\psi_B}{\partial x} = -2ik_B w_e, \tag{4.9a}$$

$$\nabla^2\psi_T - \alpha^2\psi_T - 2ik_T\frac{\partial\psi_T}{\partial x} = -2ik_T(2w_e - 4W_*), \tag{4.9b}$$

$$k_B = 1/(2\omega_B), \tag{4.9c}$$

$$k_T = 1/(2\omega_T). \tag{4.9d}$$

and where

$$\alpha^2 = F\frac{\omega_o - i\kappa}{\omega_o - i2\delta_s(1 + 2r_i/r)}. \tag{4.10}$$

We will consider forcing functions of the form

$$w_e = \sum_{n=1} w_{en}\sin(n\pi y) \qquad W_* = \sum_{n=1} W_{*n}\sin(n\pi y), \tag{4.11}$$

and so will look for solutions also in terms of a Fourier sine series. However, the boundary conditions for the streamfunction in the lower layer is not zero on the basin boundary and, in particular, not at $y = 0$ or $y = 1$. That means neither the barotropic nor, more significantly, the baroclinic streamfunction is zero at the end points of the y interval. To improve the convergence of the solution it is useful to write the solution in the form

$$\psi_T = -\Psi_2\frac{\cosh\alpha(y - 1/2)}{\cosh\alpha/2} + \sum_{n=1}\varphi_{Tn}(x)\sin(n\pi y), \tag{4.12a}$$

$$\psi_B = \hat{h}_2\Psi_2 + \sum_{n=1}\varphi_{Bn}(x)\sin(n\pi y). \tag{4.12b}$$

The forcing functions will be split into a part independent of x, representing a broad, basinwide upwelling and a part that is localized, in the present case, to a narrow region in the eastern sub-basin. That is,

$$w_{en} = w_n + V_n\delta(x - z),$$
$$W_{*n} = w_{*n} + V_{*n}\delta(x - z), \tag{4.13}$$

where z is the position of a narrow upwelling.

The Fourier amplitudes in (4.12a,b) can be found by solving the ordinary differential equations that result by inserting those representations in (4.9a,b) (the convergence of the representations allows for term-by-term differentiation). The resulting equations can be solved by standard means and the formulas for the Fourier coefficients are given in appendix A. It is important to note, by examining the results in appendix A, that the solutions depend on the, as yet, unknown values of the streamfunction Ψ_1 on the ridge segment and Ψ_2 on the outer boundary of the lower layer. Those constants are determined by the application of (3.1), the circulation constraint, and (3.2), the mass conservation condition. Since

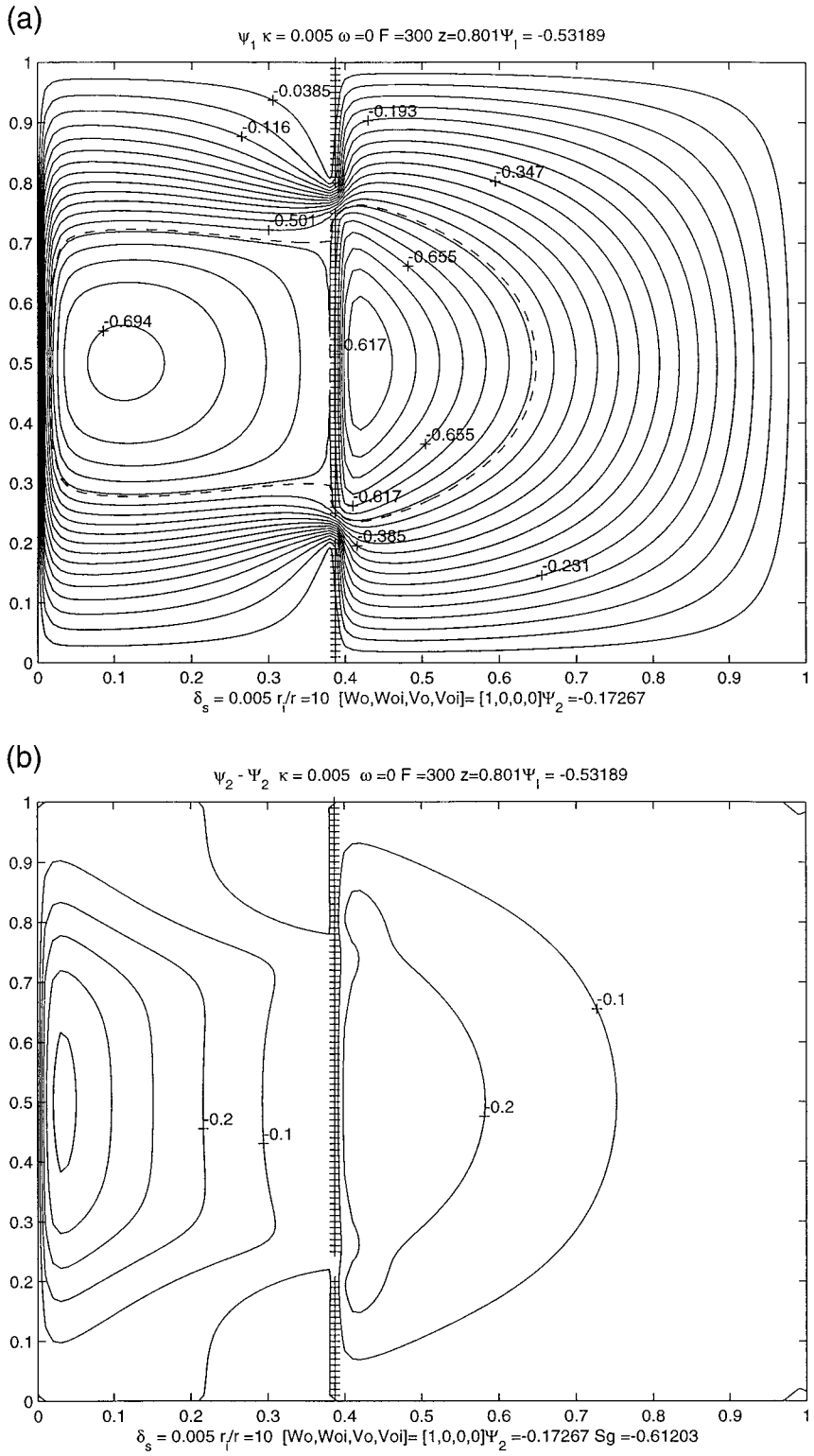

FIG. 7. The circulation pattern for the case of weak thermal damping ($\kappa = 0.005$) but strong interfacial friction between the layers ($r_i/r = 10$), $F = 300$, and $\delta_s = 0.01$. (a) The circulation in the upper layer. Note the unidirectional flow along the ridge. (b) The flow in the lower layer.

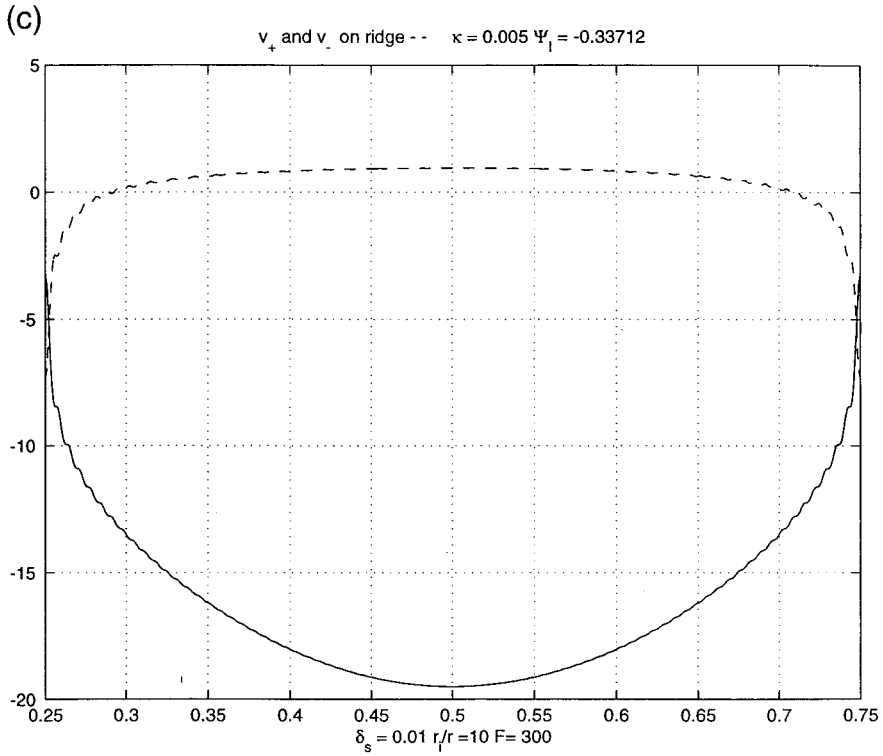

FIG. 7. (*Continued*) (c) The meridional velocity just to the east of the ridge (solid) and just to the west of the ridge (dashed).

$$\psi_1 = \psi_B + \hat{h}_2\psi_T, \tag{4.14a}$$

$$\psi_2 = \psi_B - \hat{h}_1\psi_T, \tag{4.14b}$$

one can apply the results of appendix A directly to obtain coupled equations for the streamfunction constants.

The constraint provided by the circulation integral (3.1) can be written in the form

$$c_1\Psi_I + c_2\Psi_2 = -X_c, \tag{4.15}$$

where the coefficients $c_1$and c_2, as well as the constant X_c, are given in appendix B.

The application of the mass conservation constraint in the linear limit also gives rise to a linear equation in the streamfunction constants. It is useful, however, to carry out the integrals indicated in (3.2) separately for the two adjacent sub-basins. Since the two sub-basins are joined by the single gap in the lower layer, through which an $O(b)$ flux can take place, the constraint must be applied to the sum of the two basins. However, the individual budgets will allow us to calculate the flux at higher order from one sub-basin to the next.

For simplicity, I will assume that the net $O(b)$ mass flux into the lower layer from the lateral boundary, the term denoted by S_2 in (3.2) is exactly balanced by the integral of the *imposed* cross-isopycnal flux W_*. This eliminates a mass source forcing term to the circulation and requires that the auto-induced cross-isopycnal mass flux due to the thermal dissipation integrate to zero over the whole lower layer. It is easy to relax this condition, but it would add a somewhat arbitrary forcing function to the problem.

With this simple condition imposed, the condition (3.2) in the linear limit becomes

$$\Psi_I(\mathrm{DE1} + \mathrm{DW1}) + \Psi_2(\mathrm{DE2} + \mathrm{DW2}) = -Y_c, \tag{4.16}$$

where the coefficients in (4.16) are also given in appendix B. With the solution of (4.15) and (4.16) the solutions are complete.

If the mass conservation equation is integrated only over the area of the eastern basin in the lower layer we obtain

$$\begin{aligned} S_{\mathrm{gap}} &\equiv \int_{\mathrm{gap}} u_2^{(1)}\hat{h}_2\, dy \\ &= \iint_{A_E} W_*\, dx\, dy - S_{2E} \\ &\quad - iF\hat{h}_2(\omega_o - i\kappa)\iint_{A_E}\psi_T\, dx\, dy. \end{aligned} \tag{4.17}$$

In (4.17) the flux through the gap is given in terms of the mass flux through the interface in the eastern basin (the first and third terms in the equation) minus

the flux into the *eastern* basin through its lateral boundary. The difference is the $O(b)$ mass flux from the western to eastern basin in the lower layer. Although we have applied the condition that the total mass flux through the outer boundary match the imposed cross-isopycnal upwelling, no such constraint is required for the eastern basin alone. So, depending on our specification of the local boundary mass fluxes, the flow through the gap is determined only up to that specification. I shall not discuss this in more detail since it leaves a fairly arbitrary specification of this flux possible, but it is important to note that, in general, this mass flux is different from zero even though the quasigeostrophic mass flux as determined by the streamfunction is zero in this model.

5. Results

We begin by considering the case where there is no effective coupling between the two layers. This will occur for small κF and small r_i/r. Figure 4 shows the streamline pattern for the case where the forcing consists of

$$w_e = \sin \pi y \tag{5.1}$$

with all other forcing terms set equal to zero. The nondimensional Stommel boundary layer width δ_s has been chosen as 0.01 and $\kappa F = 10^{-6}$ and $r_i/r = 0$. This makes the interface effectively rigid and slippery, so the problem reduces to that of the single-layer model studied in PPSH. We see a circulation consistent with the barotropic model of that earlier study. The circulation east of the ridge possesses a zone of trapped fluid traced by the dashed contour, and the boundary layer flow has two stagnation points at approximately $y = 0.35$ and 0.65, well short of the ends of the segment, forming the extremities of the recirculation region. The solution has been calculated directly from the complete series solution, and satisfaction of the circulation condition has been exact without assuming that only the boundary layer on the eastern side of the ridge dominates the dissipation in the solution. Nevertheless, in this case, that would be an apt description of the dynamics, again in agreement with the development described in PPSH and in agreement with the consequences of Godfrey's (1989) ''Island Rule.'' The circulation in the lower layer is essentially zero in this case and is not shown.

The situation becomes more interesting when the coupling between the layers is strong. Consider the case first when the interface is slippery, that is, when the interfacial friction coefficient, $r_I = 0$ but when the baroclinic coupling is strong. Figure 5 shows the circulation pattern for the case when $\kappa F = 300$ and δ_s is 0.01 so that δ_T is 0.003, and we are in the range where the baroclinic boundary layers have east–west symmetry (the left-hand edge of the schematic in Fig. 3).

In Fig. 5a we see the overall pattern of circulation in the upper layer and it is immediately obvious that the recirculation region, again shown by the dashed contour, has grown such that the flow along the ridge segment is all in one direction (which direction depends on the sign of the forcing; in the present case the flow is southward). Yet, with the interfacial friction equal to zero the constraint on the flow around the ridge segment given by (3.1) is simply that the total circulation around the segment between the gaps must be zero. If it were true that the only significant velocity (and dissipation) occurred on the eastern side of the island, this would appear to be inconsistent with this result and is similar to the conundrum posed by WS as described in the introduction.

Figure 5b shows a more detailed picture of the flow in the vicinity of the segment in the upper layer. The major boundary layer, as far as transport is concerned, is certainly on the eastern side in agreement with our expectations and in concordance with the requirements for the validity of the island rule. However, careful examination shows a contour encircling the western side of the segment. There is relatively little transport involved but the meridional velocity is not negligible. The contributor to this velocity on the western side of the ridge is given by the baroclinic portion of the flow shown in Fig. 5c. There is essential east–west symmetry for the baroclinic component whose characteristic length scale is $(\delta_s\delta_T)^{1/2} \sim 0.005$. The contribution that it makes to the velocity (and hence the dissipation) on the two sides of the ridge can be seen clearly in Fig. 5d, where the meridional velocity as a function of y along the ridge is shown. The upper panel shows v on the eastern side of the ridge as a solid line (note it is everywhere negative), while the dashed curve yields the meridional velocity on the western side of the ridge, also negative for all y. Their integrals over the ridge segment length balance as imposed by the constraint condition (4.15). The lower panel in the same figure shows the relative contributions of the baroclinic (dashed) and barotropic (solid) meridional velocities on the western side of the ridge and, as anticipated, it is the baroclinic contribution that produces the balancing western flow. To balance that flow a strong barotropic southward component is required on the eastern side of the ridge, which produces the flow pattern seen in Fig. 5a.

The flow in the lower layer is shown in Fig. 5e where contours of $\psi_2 - \Psi_2$ are shown in the vicinity of the ridge. It is the unidirectional flow along the ridge in the lower layer, which does not directly feel the circulation constraint, that is then communicated vertically to the upper layer. There is, in fact, no flow through the gap at lowest order [but see (4.17)] as can be verified by calculating the zonal velocity to the immediate west of the ridge (see below). In the figure only the streamline corresponding to $\psi_2 = \Psi_2$ threads through the gap.

Figure 5f shows the profile of the zonal velocity at a position, $x = 0.25$, to the west of the ridge at $x = 0.387$. Note the sharp peaks in the profiles at the latitude of the gaps in the ridge. To emphasize this the ridge and

its gaps are depicted at an arbitrary location on the right of the figure. The jets are very nearly barotropic, and it is important to note that, although the flow is toward the ridge in the south, the width of the jets decreases eastward in each jet as can be seen in Fig. 5a. To verify that there is no flow through the gaps in the lower layer at the ridge, Fig. 5g shows the same zonal velocity profiles at a position just west of the ridge. We note that the zonal velocity in the lower layer, seen in the lower panel, is now nearly zero.

Figure 6 shows the circulation pattern produced for the same parameter settings, where now the forcing is concentrated, as a delta function. That is, now

$$w_e = V = 2\sum_{n=1} e^{-(n^2 0.1)} \sin(n\pi/2)\sin(n\pi y)\delta(x - 0.5), \tag{5.2}$$

which yields a slightly modified sine profile in y with a peak forcing concentrated just east of the ridge. Figure 6a shows the circulation in the upper layer, which again is unidirectional along the ridge, a result that appears robust with this strong interlayer coupling regardless of the zonal structure of the forcing. Figure 6b shows the jets to the west of the ridge at the same position as in Fig. 5f. The structure is nearly indistinguishable, although there is a difference in amplitude. Again, the structure seems sculpted by the interaction with the ridge rather than reflecting the details of the forcing.

If the coupling between the two layers is due to friction rather than to thermal damping, a similar result, that is, the expansion of the zone of recirculation, can take place although the mechanism is different. Figure 7 shows the circulation pattern in the case where the thermal damping coefficient κ is very small (0.005) but the ratio $r_i/r = 10$. The forcing is as in (5.1). In Fig. 7a the circulation pattern of the upper layer is shown and, again, the flow along the ridge segment is unidirectional. Figure 7b shows the streamline pattern in the lower layer, and again we note that the flow is unidirectional along the peninsula connected to the northern boundary of the basin in the interval of the upper layer's ridge segment. Figure 7c shows the meridional velocity on each side of the ridge. It is clear that the circulation constraint is not achieved by balancing the integrals of v on each side of the ridge. Instead, it is the coupling term between the layers that dominates in (3.1), allowing a unidirectional flow along the ridge.

Finally, in Fig. 8 we show the result due to a purely baroclinic forcing in which w_e is zero and

$$W_* = \sin \pi y \tag{5.3}$$

with all other forcing zero. The circulation pattern in the upper layer is shown in Fig. 8a. The flow is again unidirectional along the ridge at the same parameter setting, $r_I = 0$, $\kappa F = 300$, $\delta_s = 0.01$, as in Fig. 5. The direction of the upper-layer circulation is reversed since the forcing now leads to vortex compression in the upper layer. Figure 8b shows the circulation in the lower layer. Because the forcing is baroclinic, the major baroclinic response tends to be limited to narrow boundary layers [of width $(\delta_s\delta_T)^{1/2}$] as seen in Fig. 8c. There is, however, a strong barotropic response induced by the interaction with the topography, and this barotropic component is shown in Fig. 8d. If that figure is compared with Fig. 8a, it is clear that in the western basin, and the region just to the east of the ridge segment, the circulation is barotropic and topographically generated. This is also true of the zonal jets shown in Fig. 8e, which are clearly essentially barotropic in spite of the purely baroclinic forcing. This part of the solution is due almost entirely to the first term in Eq. (A.1a), that is, the part generated by the island constant Ψ_I as a consequence of the Kelvin integral constraint (3.1). In Fig. 8f the meridional velocities on each side of the ridge segment are again shown and, again with no interfacial friction, the constraint is satisfied by the baroclinic production of meridional flow in the upper layer in the thin boundary layer to the west of the ridge.

Thus, the barotropic circulation in this parameter range, $\delta_T \leq \delta_S$, seems largely independent of the structure of the forcing. It is the interaction of the forcing and the topography, exciting a barotropic response which reaches far to the west of the ridge in the form of zonal jets, that is a strongly robust feature of the physics.

6. Summary and conclusions

In this paper we have examined the response of a quasigeostrophic, two-layer model of the steady circulation of a steady flow, driven by upwelling at the upper boundary and the interface of the two layers as a model for the circulation of the abyss in the presence of a midocean ridge. The ridge is represented by a meridional barrier pierced by two gaps. One gap extends through both layers, while the other gap is limited to the upper layer alone. The geometry of the ridge and its gaps mixes the barotropic and baroclinic responses to the forcing, and this has a fundamental effect on the resulting circulation.

The isolated segment of the model ridge in the upper layer adds an islandlike feature to the circulation, and for the quasigeostrophic model this is manifested by the need to satisfy a version of the Kelvin circulation theorem on a circuit girdling the island. When the baroclinic coupling between the two layers is strong enough, the recirculation region in the upper layer grows in size beyond what its extent would be for a barotropic fluid to such an extent that the flow along the eastern flank of the ridge becomes unidirectional. This single direction of flow, which had been observed by Warren and Speer (1991), can be traced back to the important role of the baroclinic response of the fluid to the upwelling forcing. The baroclinic response for small deformation radius and $O(1)$ thermal damping (in the sense that a baroclinic Rossby wave would damp on the timescale

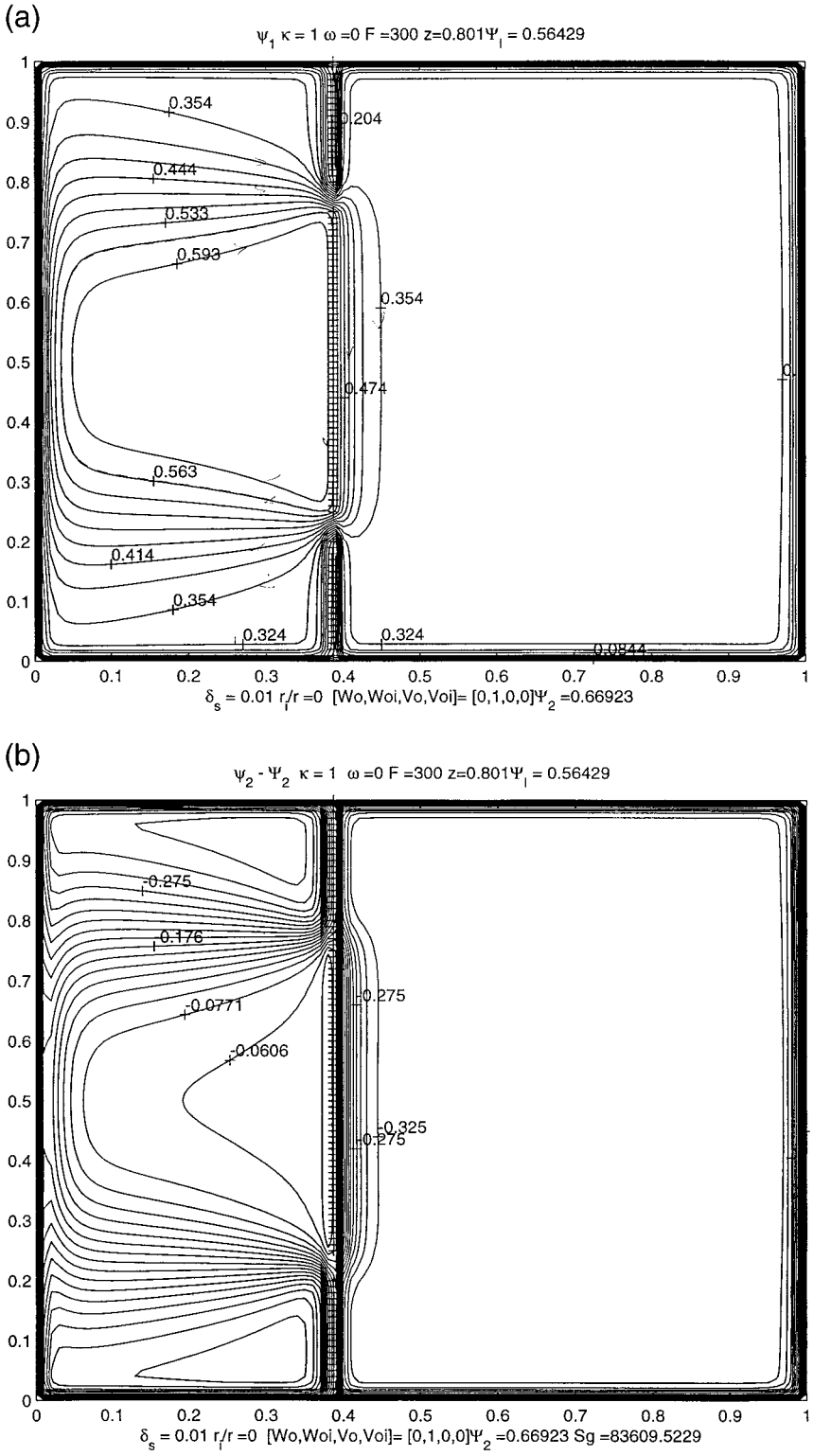

FIG. 8. The circulation produced by a purely baroclinic forcing due to a $\sin \pi y$ cross-isopycnal flow at the interface between the two layers. (a) The circulation in the upper layer. (b) The circulation in the lower layer.

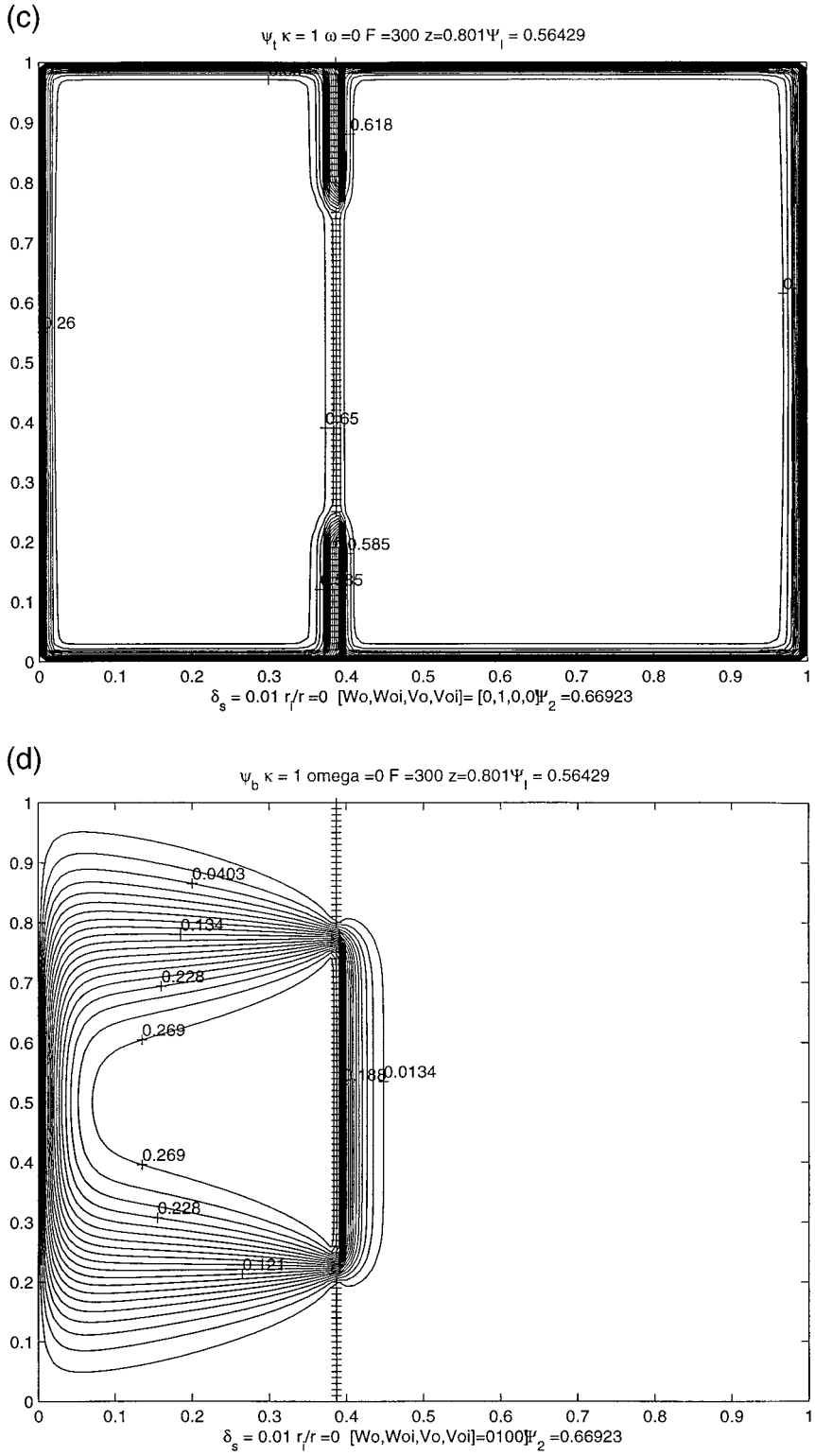

FIG. 8. (*Continued*) (c) The baroclinic response demonstrating that the major baroclinic response occurs in narrow boundary layers. (d) The barotropic portion of the circulation.

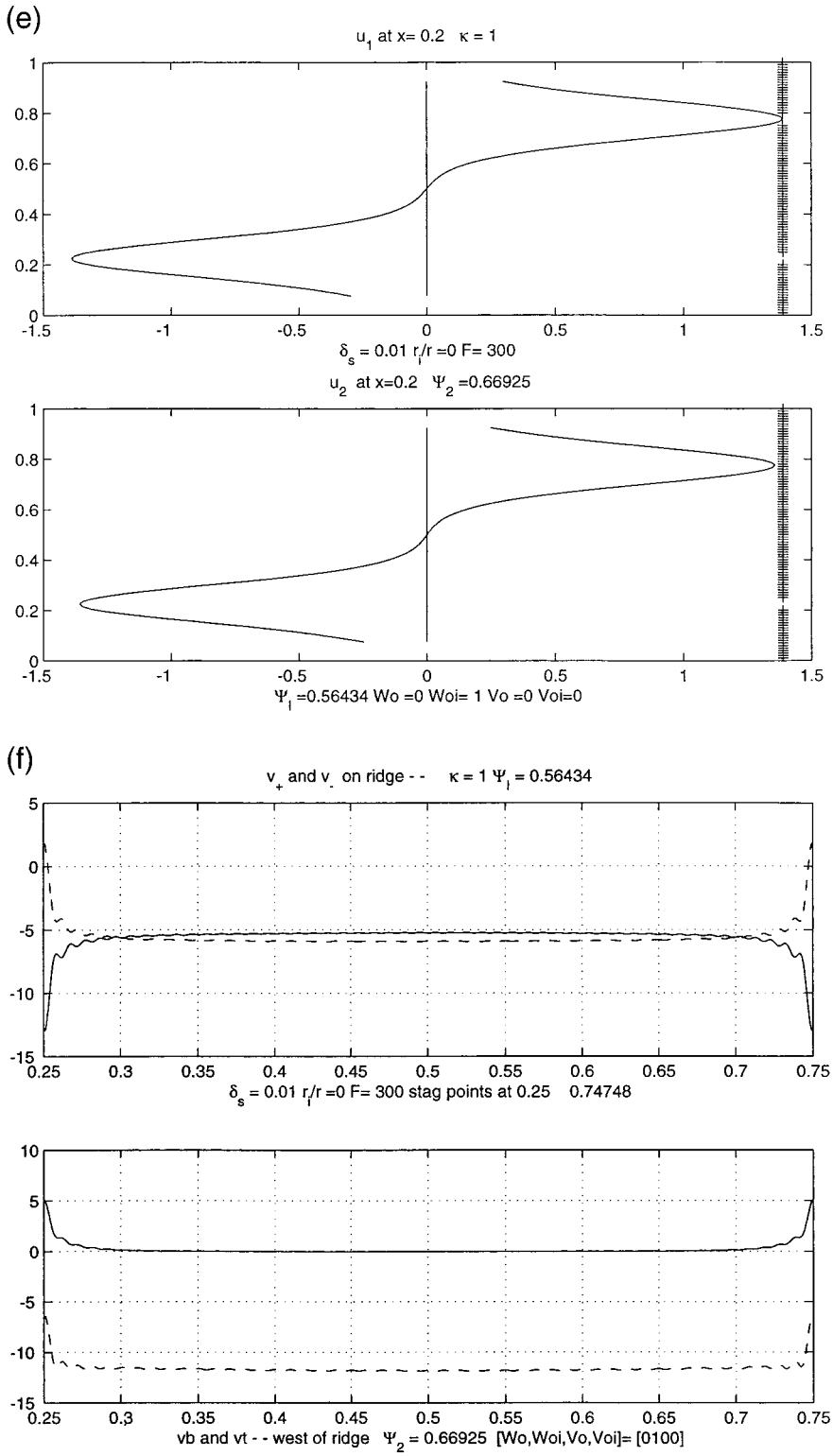

FIG. 8. (*Continued*) (e) The *barotropic* zonal jets that are produced west of the ridge. (f) The meridional velocity on each side of the ridge. Upper panel shows v to the east of the ridge (solid curve) and v to the west of the ridge (dashed curve). Lower panel the barotropic (solid curve) and baroclinic (dashed) meridional velocities just west of the ridge.

of its period) is limited to narrow zones near all solid boundaries, both east and west of the ridge. Although the major currents, in terms of transport, are east of the ridge due to the dynamical asymmetry associated with the β effect, there is sufficient velocity in the narrow baroclinic boundary layer to the west of the ridge to balance the dissipation of the unidirectional barotropic velocity east of the ridge to satisfy the Kelvin constraint (3.1).

Very strong interfacial frictional coupling provides an alternative mechanism to allow the growth of the eastern zone of recirculation near the isolated ridge segment, producing unidirectional flow along the ridge. In this case there is no longer the constraint that the meridional average of v be equal on each side of the ridge. Indeed, in the limit of very large frictional coupling the requirement of (3.1) is simply that the upper-layer meridional velocity have a y average equal to that of the lower layer in the latitude band of the ridge segment. The fact that the lower-layer ridge does not form an isolated segment easily allows unidirectional flow in the lower layer, and the frictional coupling projects that flow upward into the upper layer.

Of course, this model is highly simplified. Both the coupling mechanisms, the thermal damping and the interfacial frictional coupling, are poor representations of rather more complicated turbulent processes of mixing of momentum and density. The nature of the interfacial friction in the model, serving as it does to smooth out the vertical shear of the mean flow, might be thought of as a crude representation of the reduction in vertical shear due to baroclinic instability not resolved by the calculation. It is important to be able to think of the coupling process that way rather than the simple effect of Ekman layers at the interface between the two layers since in that case the ratio r_i/r is fixed at a value of 0.5 while a much stronger value of the order (10) is required to produce unidirectional flow along the ridge. If r is thought of as a measure of the in-layer dissipation of momentum due to lateral shear instabilities and r_I is a measure of baroclinic instability, the ratio may be much larger than one, at least locally.

It is hard to argue for a particular value of κ, and in this paper I have chosen a value in order that the major baroclinic response is limited to narrow boundary layers around the basin and on the ridge so that the baroclinic response is not much broader than a deformation radius. This, and the timescale for wave decay that it implies, is an arbitrary choice at this point, but a smaller value of κ can be offset by a larger value of F in the theory.

One of the more robust results of the theory is the prediction of essentially barotropic jets in the region west of the forcing. The barotropic nature of the jet response is largely independent of the structure of the forcing, that is, whether that forcing is barotropic or baroclinic or some combination. It is the interaction of the flow with the ridge and its gaps that excites the jets. That has been seen earlier in barotropic models (e.g., PPSH) but it appears to be a robust response in a baroclinic model as well. The width of the zonal flow depends strongly on the degree of friction in the model. For the simple frictional parameterization of this model the width of the zonal jets is $(\delta_s[x_T - x])^{1/2}$, where δ_s is Stommel's boundary layer thickness and $x_T - x$ is the distance west of the ridge placed at x_T. Other parameterizations of mixing, for example, lateral mixing, would give different rules for the spreading of the widths of the zonal flows as a function of distance to the west. Indeed, if the momentum mixing is strong enough, the widths of the regions of zonal flow may be so broad as to bring into question the adjectival ''jet.'' For example, the zonal flows in Fig. 5f already extend over almost half the width of the basin well west of the jet and squeeze down to the widths of the gaps only quite near the ridge, as seen in Fig. 5g. Hogg and Owens (1999) in their analysis of the deep circulation within the Brazil Basin point out, from float data, a strikingly stable zonal flow at about 22°S just at the latitude of the Rio de Janeiro fracture zone in the Mid-Atlantic Ridge. The data are too sparse to decide whether the current is indeed a flow through the gap. It is possible it may join, east of the ridge, the Namib Col current that Warren and Speer (1991) (see also Speer et al. 1995) have associated with a similar gap in the Walvis Ridge even farther eastward. At this point I can only argue that it is suggestive that the zonal flow lines up with the gap in a manner consistent with the theory presented above.

From a fluid dynamical point of view the major result is that baroclinicity, while of course not vitiating the validity of Kelvin's circulation theorem, makes its application more complex in the steady state. That the narrow baroclinic boundary currents introduce important contributions to the resulting dissipation integral due to the flow to the west of the ridge segment means that the assumptions required for the validity of Godfrey's Island Rule will no longer be satisfied. This emphasizes the importance of the original constraint, which is the circulation integral of the momentum equation around the ridge segment itself.

Acknowledgments. This research was supported in part by National Science Foundation Grant OCE 9901654. The author is grateful to Breck Owens and Nelson Hogg for helpful guidance concerning the Brazil Basin experiment and to Bruce Warren for stubbornly insisting that the observed flow along the ridge in the Angola Basin required serious theoretical consideration.

APPENDIX A

Fourier Coefficients for (4.12a,b)

The Fourier coefficients for the solution as a sine series given by (4.12a,b) can be shown to be
For the barotropic mode:

$x \geq x_T$

$$\varphi_{Bn} = \hat{h}_1 \Psi_I g_{n2} \frac{\sin a_n(x - x_e)}{\sin a_n(x_T - x_e)} e^{ik_B(x-x_T)} + \frac{2ik_B w_n}{n^2\pi^2}\left[1 - \frac{\sin a_n(x - x_e)}{\sin a_n(x_T - x_e)} e^{ik_B(x-x_T)} - \frac{\sin a_n(x - x_T)}{\sin a_n(x_T - x_e)} e^{ik_B(x-x_e)}\right]$$
$$+ \frac{2ik_B V_n}{a_n \sin a_n(x_T - x_e)}[\sin a_n(z - x_T) \sin a_n(x - x_e) e^{ik_B(x-z)}\Theta(x - z)$$
$$+ \sin a_n(z - x_e) \sin a_n(x - x_T) e^{ik_B(x-z)}\Theta(z - x)], \tag{A.1a}$$

$x \leq x_T$

$$\varphi_{Bn} = \hat{h}_1 \Psi_I g_{n2} \frac{\sin a_n(x - x_w)}{\sin a_n(x_T - x_w)} e^{ik_B(x-x_T)} + \frac{2ik_B w_n}{n^2\pi^2}\left[1 - \frac{\sin a_n(x - x_w)}{\sin a_n(x_T - x_w)} e^{ik_B(x-x_T)} - \frac{\sin a_n(x - x_T)}{\sin a_n(x_T - x_w)} e^{ik_B(x-x_w)}\right]. \tag{A.1b}$$

Here x_e and x_w are the eastern and western coordinates of the meridional boundaries of the basin. The constant a_n is defined as

$$a_n = (k_B^2 - n^2\pi^2)^{1/2}, \quad \text{and} \tag{A.2a}$$

$$g_{n2} = \frac{2}{dn^2\pi^2}[\sin n\pi(y_s + d) - \sin n\pi y_s - \sin n\pi y_n + \sin n\pi(y_n + d)]. \tag{A.2b}$$

In (A.1a) the function $\Theta(\xi)$ is the Heavyside step function, which is unity for positive values of its argument and zero when its argument is negative.

For the baroclinic portion of the solution,

$x \geq x_T$

$$\varphi_{Tn} = \Psi_I g_{n2} \frac{\sin b_n(x - x_e)}{\sin b_n(x_T - x_e)} e^{ik_T(x-x_T)} + \Psi_2 g_{n1}\left[\frac{\sin b_n(x - x_T)}{\sin b_n(x_T - x_e)} e^{ik_T(x-x_e)} - \frac{\sin b_n(x - x_e)}{\sin b_n(x_T - x_e)} e^{ik_T(x-x_T)}\right]$$
$$+ \frac{4ik_T(w_n - 2w_{*n})}{k_T^2 - b_n^2}\left[1 + \frac{\sin b_n(x - x_T)}{\sin b_n(x_T - x_e)} e^{ik_T(x-x_e)} - \frac{\sin b_n(x - x_e)}{\sin b_n(x_T - x_e)} e^{ik_T(x-x_T)}\right]$$
$$+ \frac{4ik_T(V_n - 2V_{*n})}{b_n \sin b_n(x_T - x_e)}[\sin b_n(z - x_T) \sin b_n(x - x_e) e^{ik_T(x-z)}\Theta(x - z)$$
$$+ \sin b_n(z - x_e) \sin b_n(x - x_T) e^{ik_T(x-z)}\Theta(z - x)], \tag{A.3a}$$

while

$x \leq x_T$

$$\varphi_{Tn} = \Psi_I g_{n2} \frac{\sin b_n(x - x_w)}{\sin b_n(x_T - x_w)} e^{ik_T(x-x_T)} + \Psi_2 g_{n1}\left[\frac{\sin b_n(x - x_T)}{\sin b_n(x_T - x_w)} e^{ik_T(x-x_w)} - \frac{\sin b_n(x - x_w)}{\sin b_n(x_T - x_w)} e^{ik_T(x-x_T)}\right]$$
$$+ \frac{4ik_T(w_n - 2w_{*n})}{k_T^2 - b_n^2}\left[1 + \frac{\sin b_n(x - x_T)}{\sin b_n(x_T - x_w)} e^{ik_T(x-x_w)} - \frac{\sin b_n(x - x_w)}{\sin b_n(x_T - x_w)} e^{ik_T(x-x_T)}\right], \tag{A.3b}$$

where

$$b_n = \{k_T^2 - n^2\pi^2 - F - 2ik_T F[2\delta_s(1 + 2r_i/r) - \kappa]\}^{1/2} \tag{A.4a}$$

$$g_{n1} = \frac{2\alpha[1 - (-1)^n]}{n\pi(n^2\pi^2 + \alpha^2)}. \tag{A.4b}$$

APPENDIX B

Coefficients for the Integral Constraints

By applying the circulation integral to the ridge segment in the upper layer, Eq. (4.15) is obtained, in which the coefficients can be shown to be

$$c_1 = \sum_{n=1} a_n g_{n3} g_{n2} \hat{h}_1 [\cot a_n(x_T - x_e) - \cot a_n(x_T - x_w)] + b_n \frac{\omega_T}{\omega_B} g_{n3} g_{n2} [\cot b_n(x_T - x_e) - \cot b_n(x_T - x_w)] \quad \text{(B.1a)}$$

$$c_2 = \sum_{n=1} g_{n3} g_{n1} \hat{h}_2 b_n \frac{\omega_T}{\omega_B} \left\{ \frac{e^{-ik_T(x_e - x_T)}}{\sin b_n(x_t - x_e)} - \frac{e^{-ik_T(x_w - x_T)}}{\sin b_n(x_t - x_w)} - \cot b_n(x_T - x_e) + \cot b_n(x_T - x_w) \right\}, \quad \text{and} \quad \text{(B.1b)}$$

$$X_c = \sum_{n=1} \frac{\omega_T}{\omega_B} b_n g_{n3} \hat{h}_2 4ik_T \frac{(w_n - 2w_{*n})}{k_T^2 - b_n^2} \left[\frac{e^{-ik_T(x_e - x_T)}}{\sin b_n(x_T - x_e)} - \frac{e^{-ik_T(x_w - x_T)}}{\sin b_n(x_T - x_w)} + \cot b_n(x_T - x_w) - \cot b_n(x_T - x_e) \right]$$
$$+ \sum_{n=1} g_{n3} 2ik_B V_n e^{-ik_B(z - x_T)} \frac{\sin a_n(z - x_e)}{\sin a_n(x_T - x_e)} + \frac{\omega_T}{\omega_B} \sum g_{n3} \hat{h}_2 4ik_T (V_n - 2V_{*n}) \frac{\sin b_n(z - x_e)}{\sin b_n(x_T - x_e)} e^{-ik_T(z - x_T)} \quad \text{(B.1c)}$$

where

$$g_{n3} = \frac{1}{n\pi} \{\cos n\pi(y_s + d) - \cos n\pi(y_n - d)\}. \quad \text{(B.2)}$$

The coefficients in (4.16) are

$$\text{DE1} = \sum_{n=1} \frac{\mu_n g_{n2}}{\sin b_n(x_T - x_e)} \left\{ \frac{b_n}{k_T^2 - b_n^2} [e^{ik_T(x_e - x_T)} - \cos b_n(x_T - x_e)] + \frac{ik_T \sin b_n(x_T - x_e)}{k_T^2 - b_n^2} \right\} \quad \text{(B.3a)}$$

$$\text{DE2} = \left\{ \frac{-2}{\alpha}(x_e - x_T) \tanh\left(\frac{\alpha}{2}\right) + \sum_{n=1} \frac{2\mu_n g_{n1} b_n}{\sin b_n(x_T - x_e)} [\cos b_n(x_T - x_e) - \cos k_T(x_T - x_e)] \right\} \quad \text{(B.3b)}$$

$$\text{DW1} = \sum_{n=1} \frac{\mu_n g_{n2}}{\sin b_n(x_T - x_w)} \left\{ \frac{b_n}{k_T^2 - b_n^2} [e^{ik_T(x_w - x_T)} - \cos b_n(x_T - x_w)] + \frac{ik_T \sin b_n(x_T - x_w)}{k_T^2 - b_n^2} \right\} \quad \text{(B.3c)}$$

$$\text{DW2} = \left\{ \frac{-2}{\alpha}(x_T - x_w) \tanh\left(\frac{\alpha}{2}\right) + \sum_{n=1} \frac{2\mu_n g_{n1} b_n}{\sin b_n(x_T - x_w)} [\cos b_n(x_T - x_w) - \cos k_T(x_T - x_w)] \right\}, \quad \text{(B.3d)}$$

while

$$Y_c = \sum_{n=1} \frac{4ik_T(w_n - 2w_{*n})}{k_T^2 - b_n^2} \left\{ x_e - x_T + \frac{2b_n[\cos b_n(x_T - x_e) - \cos k_T(x_T - x_e)]}{(k_T^2 - b_n^2) \sin b_n(x_T - x_e)} \right\}$$
$$+ \sum_{n=1} \frac{4ik_T(V_n - 2V_{*n})}{(k_T^2 - b_n^2) \sin b_n(x_T - x_e)} \{\sin b_n(x_T - x_e) + e^{ik_T(x_e - z)} \sin b_n(z - x_T) - e^{ik_T(x_T - z)} \sin b_n(z - x_e)\}$$
$$+ \sum_{n=1} \frac{4ik_T(w_n - 2w_{*n})}{k_T^2 - b_n^2} \left\{ x_T - x_w + \frac{2b_n[\cos b_n(x_T - x_w) - \cos k_T(x_T - x_w)]}{(k_T^2 - b_n^2) \sin b_n(x_T - x_w)} \right\}, \quad \text{(B.3e)}$$

where $\mu_n = (1 - (-1)^n)$.

REFERENCES

Godfrey, J. S., 1989: A Sverdrup model of the depth-integrated flow from the world ocean allowing for island circulations. *Geophys. Astrophys. Fluid Dyn.,* **45,** 89–112.

Hogg, N. G., and W. B. Owens, 1999: Direct measurement of the deep circulation in the Brazil Basin. *Deep-Sea Res. II,* **46,** 335–353.

Kawase, M., 1987: Establishment of deep oceanic circulation driven by deep-water production. *J. Phys. Oceanogr.,* **17,** 2294–2317.

McWilliams, J. C., 1977: A note on a consistent quasi-geostrophic model in a multiply connected domain. *Dyn. Atmos. Oceans,* **5,** 427–442.

Pedlosky, J., 2000: The transmission and transformation of baroclinic Rossby waves by topography. *J. Phys. Oceanogr.,* **30,** 3077–3101.

——, and M. A. Spall, 1999: Rossby normal modes in basins with barriers. *J. Phys. Oceanogr.,* **29,** 2332–2349.

——, L. J. Pratt, M. A. Spall, and K. R. Helfrich, 1997: Circulation around islands and ridges. *J. Mar. Res.,* **55,** 1199–1251.

Speer, K. G., G. Siedler, and L. Talley, 1995: The Namib Col current. *Deep-Sea Res.,* **42,** 1933–1950.

Warren, B. A., and K. G. Speer, 1991: Deep circulation in the eastern South Atlantic Ocean. *Deep-Sea Res.,* **38**(Suppl.), S281–S322.